Table 2 Summary of partial dryout test results[a]

Test 1		Test 2		Test 3	
f, Hz	T_e, °C	f, Hz	T_e, °C	f, Hz	T_e, °C
0	42.8	0	42.5	0	42.8
0.05	97.0	0.15	42.3	0.2	42.3
0.1	75.1	0.1	54.7	0.15	42.3
0.15	67.8	0.05	99.4	0.1	54.0
0.2	66.6	0.1	74.2	0.05	97.0
——	——	——	——	0.1	75.1

[a] Q_e = 137 W and T_c = 20°C.

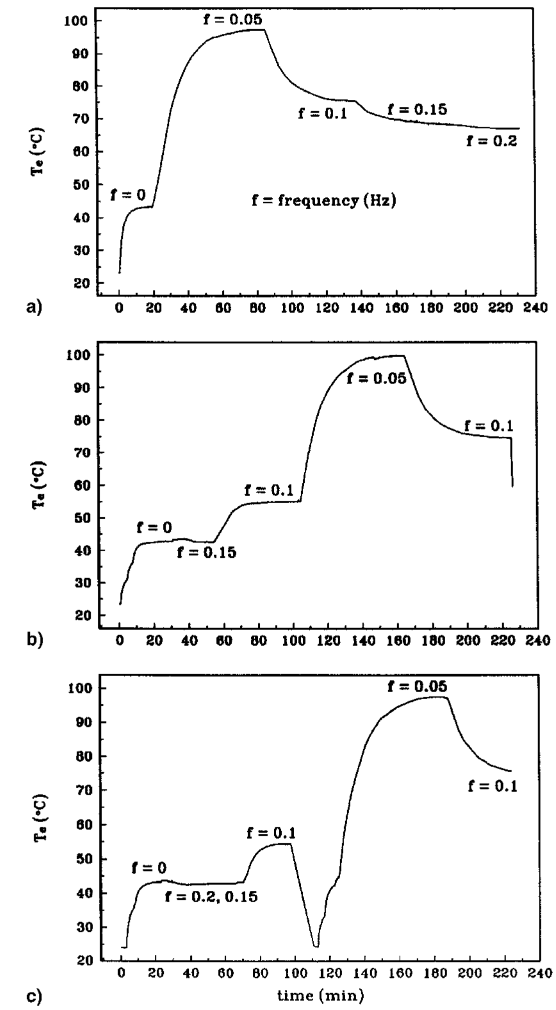

Fig. 3 Temperature vs time for the heat pipe under different dryout conditions: a) test 1, increasing frequency; b) test 2, decreasing, then increasing; and c) test 3, decreasing, allowing to reprime, then increasing.

sistance of the flexible copper-water heat pipe is dependent on the partial dryout status of the evaporator section prior to changing the frequency of the acceleration field.

Conclusions

The quasi-steady-state thermal resistance of a flexible copper-water heat pipe under varying acceleration loadings has been determined experimentally. It was found that the thermal resistance of the heat pipe is a function of the sinusoidal frequency of the acceleration field, the heat input, the condenser temperature, and the dryout condition prior to changing the acceleration frequency. To determine the feasibility of using heat pipes in transient acceleration fields, the expected frequencies and heat inputs must be known. It was determined that increasing the condenser sink temperature will decrease the thermal resistance considerably by avoiding a partial dryout situation. While the imposed acceleration field increased the heat pipe thermal resistance, the performance was improved at higher frequencies.

Acknowledgment

The authors acknowledge the support of the U.S. Air Force Office of Scientific Research under Contract F49620-93-C-0063.

References

[1]Gernert, N., et al., "Flexible Heat Pipe Cold Plates for Aircraft Thermal Control," *Proceedings of the Aerospace Technology Conference and Exposition*, 1991.

[2]Yerkes, K., and Beam, J., "Arterial Heat Pipe Performance in a Transient Heat Flux and Body Force Environment," *Proceedings of the Aerospace Atlantic Conference* (Dayton, OH), Society of Automotive Engineers, Warrendale, PA, 1992.

[3]Yerkes, K., and Hager, B., "Transient Response of Heat Pipes for Actuator Thermal Management," *Proceedings of the Aerospace Atlantic Conference* (Dayton, OH), Society of Automotive Engineers, Warrendale, PA, 1992.

[4]Faghri, A., *Heat Pipe Science and Technology*, Taylor and Francis, Washington, DC, 1994.

[5]Dunn, P., and Reay, D., *Heat Pipes*, 3rd ed., Pergamon, Oxford, England, UK, 1982.

[6]Chi, S., *Heat Pipe Theory and Practice*, Hemisphere, Washington, DC, 1976.

Double-Diffusive Convection in a Porous Trapezoidal Enclosure with Oblique Principal Axes

Hoa D. Nguyen,* Seungho Paik,*
and Rod W. Douglass†
Idaho National Engineering Laboratory,
Idaho Falls, Idaho 83415-3808

Nomenclature

B = buoyancy ratio
L_b = length of the bottom wall
L_t = length of the top wall
S^* = concentration
T^* = temperature
t = time
γ = angle formed by the base and the sidewall
θ = oblique angle
σ = specific heat ratio
ϕ = porosity

I. Introduction

DOUBLE diffusion is a buoyancy-driven convective phenomenon that has been a topic of numerous studies; however, very few have concerned anisotropic systems.[1] Of theoretical significance are the works of Kvernvold and Tyvand[2] and Tyvand,[3] in which the criteria for the onset of thermal convection and thermohaline convection, respectively, were derived for an unbounded saturated porous layer. More recently, Nilsen and Storesletten[4] conducted a similar analysis on convection in a horizontal porous channel. Kimura and Ma-

Received Oct. 26, 1995; revision received Nov. 20, 1996; accepted for publication Nov. 20, 1996.

*Staff Engineer, P.O. Box 1625, M/S 3808.
†Consulting Engineer, P.O. Box 1625, M/S 3808.

suda[5] reported solutions for small Rayleigh numbers on thermal convection in a square porous enclosure with heating from the side. Chang and Lin[6] performed full numerical simulations for a rectangular cavity including wall conduction effects. Chang and Hsiao[7] investigated the heat transfer inside a vertical porous cylinder subjected to heating along the top as well as the vertical walls. A more complex situation involving a cavity filled with two anisotropic porous layers was studied by Nguyen et al.[8] for different arrangements of boundary conditions to represent opposing diffusion, aiding diffusion, and cross diffusion with stabilizing and destabilizing concentration fields.

All of the previous studies share one common feature in that the principal axes of the permeability tensor coincide with the gravity vector. When such an alignment fails, the oblique angle could play a major role in the transport process. Tyvand and Storesletten[9] revisited the problem previously considered by Kvernvold and Tyvand,[2] but with an allowance of an arbitrary oblique angle of the principal axes. Numerical studies on this problem have been undertaken for a square enclosure with the bottom wall heated and the sidewalls insulated,[10] a rectangular enclosure with heating from the side,[11] and a horizontal annulus.[12] They all confirmed a strong influence of the anisotropy and the oblique angle. Although much has been learned, the results cannot be extrapolated because of the multiple time and length scales associated with double diffusion. Thus, the purpose of this Note is to extend the analysis to double-diffusive systems and to examine the geometry dependence thereon. The configuration to be considered is a trapezoid for which the inclination angle has been found to strongly dictate the nature of thermosolutal convection in clear fluids.[13]

II. Governing Equations

Consider a trapezoidal enclosure filled with an anisotropic porous material whose permeability $\bar{\bar{K}}$ is assumed to be of the form

$$\bar{\bar{K}} = K_1 \boldsymbol{i}'\boldsymbol{i}' + K_2 \boldsymbol{j}'\boldsymbol{j}' \tag{1}$$

where $\boldsymbol{i}'$ and $\boldsymbol{j}'$ are the unit vectors representing the principal axes and K_1 and K_2 are the principal permeabilities. In the nonprimed coordinate system, the inverse of $\bar{\bar{K}}$ becomes

$$\bar{\bar{K}} = \frac{1}{K_2}\begin{bmatrix} k_{xx}(R, \boldsymbol{\theta}) & k_{xy}(R, \theta) \\ k_{yx}(R, \theta) & k_{yy}(R, \theta) \end{bmatrix} \tag{2}$$

where $R = K_2/K_1$ and θ is formed by the $\boldsymbol{i}'$ vector and the horizontal axis. Explicit formulas for the tensor components are available elsewhere.[10]

By making use of the definition of the stream function $\boldsymbol{\psi}^*$, the governing equations can be expressed in nondimensional form as

$$k_{xx}\frac{\partial^2 \boldsymbol{\psi}^*}{\partial x^{*2}} + 2k_{xy}\frac{\partial^2 \psi^*}{\partial x^* \partial y^*} + k_{yy}\frac{\partial^2 \psi^*}{\partial y^{*2}} = -Ra\left[\frac{\partial T^*}{\partial x^*} - B\frac{\partial S^*}{\partial x^*}\right] \tag{3}$$

$$\sigma\frac{\partial T^*}{\partial t^*} + \frac{\partial \psi^*}{\partial y^*}\frac{\partial T^*}{\partial x^*} - \frac{\partial \psi^*}{\partial x^*}\frac{\partial T^*}{\partial y^*} = \frac{\partial^2 T^*}{\partial x^{*2}} + \frac{\partial^2 T^*}{\partial y^{*2}} \tag{4}$$

$$\boldsymbol{\phi}\frac{\partial S^*}{\partial t^*} + \frac{\partial \psi^*}{\partial y^*}\frac{\partial S^*}{\partial x^*} - \frac{\partial \psi^*}{\partial x^*}\frac{\partial S^*}{\partial y^*} = \frac{1}{Le}\left[\frac{\partial^2 S^*}{\partial x^{*2}} + \frac{\partial^2 S^*}{\partial y^{*2}}\right] \tag{5}$$

in which a Cartesian frame of reference has been adopted with its origin located at the intersection of the diagonals and the x and y axes aligned in the horizontal and vertical axes, respectively. The variables were made dimensionless by using the following scales:

$$t^* = \frac{\alpha t}{L_b^2}, \quad (x^*, y^*) = \frac{(x, y)}{L_b}, \quad \psi^* = \frac{\psi}{\alpha}, \quad Le = \frac{\alpha}{D}$$
$$Ra = \frac{K_2 \boldsymbol{\beta}_T g L_b (T_1 - T_0)}{\alpha\nu}, \quad B = \frac{\beta_S(S_1 - S_0)}{\beta_T(T_1 - T_0)} \tag{6}$$
$$\sigma = \frac{\phi(\rho c)_f + (1-\phi)(\rho c)_s}{(\rho c)_f}, \quad S^* = \frac{S - S_0}{S_1 - S_0}, \quad T^* = \frac{T - T_0}{T_1 - T_0}$$

where c is the specific heat, g is the gravity, α is the effective thermal diffusion coefficient, β is the expansion coefficient, ν is the kinematic viscosity, and ρ is the density. The subscripts f, s, S, and T pertain to fluid, solid, concentration, and temperature, in respective order. Note that several assumptions have been invoked into the previous mathematical model, including Darcian flow, local thermal equilibrium, negligible dispersion, and Boussinesq approximations.

The constraints imposed on Eqs. (3–5) are 1) $S^* = 1$ and $T^* = 1$ along the left sidewall; 2) $S^* = 0$ and $T^* = 0$ along the right sidewall; and 3) $\partial S^*/\partial y = 0$ and $\partial T^*/\partial y = 0$ on the top and bottom walls, with $S^* = 0$ and $T^* = 0$ as the initial conditions.

III. Results and Discussion

Solutions were obtained by a Galerkin-based finite element method in conjunction with a semi-implicit method, which treats the convection terms and the diffusion terms by the second-order Adams–Bashforth and Crank–Nicolson schemes, respectively. Unless otherwise stated, the results presented in this section are based on the following sets of geometric parameters: $L_t = 0.5$, $L_b = 1.0$, and $\gamma = \pi/3$; physical parameters:

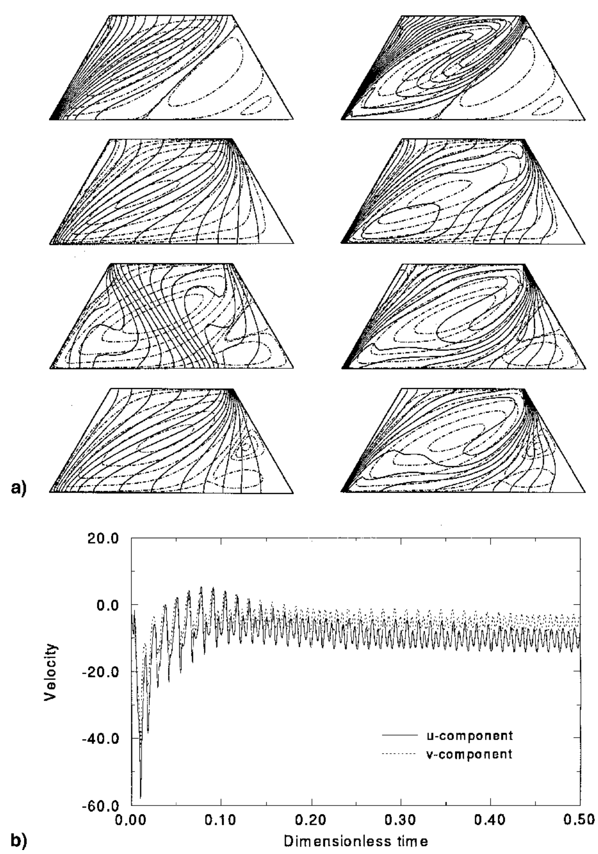

Fig. 1 Evolution of double-diffusive convection: a) isotherms (left) and isoconcentrations (right) at t^* = 0.01, 0.1, 0.3, and 0.5 from top to bottom and b) velocity at origin.

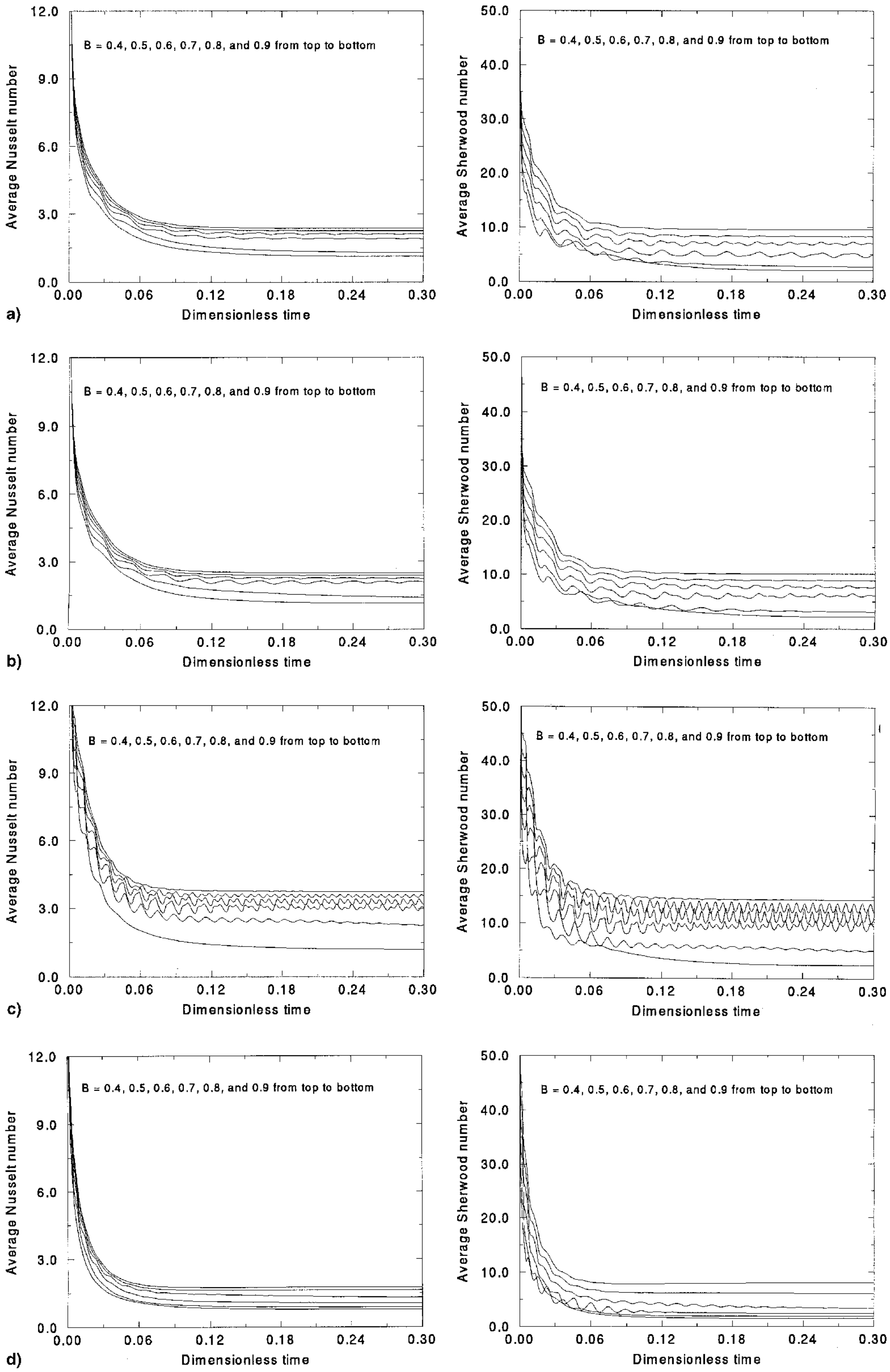

Fig. 2 Heat and mass transfer rates: a) R = 0.5, $\theta = \pi/4$, and $\gamma = \pi/3$; b) R = 0.5, $\theta = \pi/3$, and $\gamma = \pi/3$; c) R = 0.1, $\theta = \pi/3$, and $\gamma = \pi/3$; and d) R = 0.1, $\theta = \pi/3$, and $\gamma = \pi/4$.

Ra = 100, Le = 10, B = 0.7, R = 0.1, σ = 1.0, ϕ = 0.3, and $\theta = \pi/3$; and discretization parameters: $\Delta t = 10^{-5}$ and a 41 $\times$ 41 nonuniform mesh with element sizes distributed according to the Gauss–Lobatto quadrature points.

Figure 1a shows the temperature and concentration fields superimposed on the streamlines depicted at t^* = 0.01, 0.1, 0.3, and 0.5 from the top to the bottom. At first glance, it is noticed that at t^* = 0.01 flow currents have already gained sufficient strength to produce remarkable effects in the temperature field as reflected by the deformation of isotherms from what would otherwise be straight lines. This is even more so in the concentration field where mass diffusion is 10 times slower than thermal diffusion, i.e., Le = 10. As the process evolves further in time, the lower right-hand corner of the stagnant region seen at t^* = 0.01 develops into a complex secondary vortex system, whereas the isotherms and the isoconcentrations appear to be oscillating. Such oscillatory behavior becomes obvious by noting the repetitive pattern of the